J|A|C|S
ARTICLES
Published on Web 04/20/2007

Selective Bond Breaking in β-D-Ribose by Gas-Phase Electron Attachment around 8 eV

Isabella Baccarelli,[†] Franco A. Gianturco,*[,‡] Andrea Grandi,[†] Nico Sanna,[†] Robert R. Lucchese,[§] Ilko Bald,[||] Janina Kopyra,[||,#] and Eugen Illenberger[||]

Contribution from the CASPUR, Supercomputing Consortium, via de' Tizii 6, 00185 Rome, Italy, Department of Chemistry and CNISM, University of Rome La Sapienza, Piazzale A. Moro 5, 00185 Rome, Italy, Department of Chemistry, Texas A&M University, College Station, Texas 77843-3255, and Institut fuer Chemie und Biochemie, Physikalische und Theoretische Chemie, Freie Universitaet Berlin, Takustrasse 3, 14195 Berlin, Germany

Received January 24, 2007; E-mail: fa.gianturco@caspur.it

Abstract: Electron attachment experiments are carried out on the β-D-ribose molecule in the gas phase for the energy region around 8 eV, and clear fragmentation products are observed for different mass values. A computational analysis of the relevant dynamics is also carried out for the β-D-ribose in both the furanosic and pyranosic form as gaseous targets around that energy range. The quantum scattering attributes obtained from the calculations reveal in both systems the presence of transient negative ions (TNIs). An analysis of the spatial features of the excess resonant electron, together with the computation and characterization of the target molecular normal modes, suggests possible break-up pathways of the initial, metastable molecular species.

1. Introduction

The properties and the chemistry of carbohydrates are nowadays widely recognized for the important role they play in several biological processes and in industrial applications.[1] Monosaccharides are the basic units and building blocks of carbohydrates and two of them, the 2-deoxy-D-ribose and the D-ribose, also occupy a central position in the chemical structure of, respectively, the deoxyribonucleic acid (DNA) and the ribonucleic acid (RNA) by binding the phosphate groups into the formation of the well-known backbone structures which provide a link between neighboring nucleotides bases of the single strand of DNA.

Recent years have witnessed a remarkable growth of both experimental and theoretical investigations which employ low-energy electrons as probes of the various DNA building blocks in the gas-phase: one important motivation of such studies resides on their providing nanoscopic information when real biosystems are exposed to ionizing radiation and can undergo irreversible molecular damage.[2−4] Possible effects induced by low-energy electrons to DNA or to RNA strands could be also thought of as preferentially starting at the sugar backbone; hence the backbone, or the sugar itself, could be identified as important electron attachment sites leading to strand breaks or as intermediate in producing strand breaks.

There is a variety of processes initiated by the primary radiation impinging on DNA which can induce serious genetic effects, such as mutation.[2] The nanoscopic mechanism which has reached by now a rather broad consensus in the relevant literature[3−8] involves the initial removal of electrons from the molecular components of the complex network by the impinging radiation. Such electrons originate from either the valence levels of the chemical bonds or from the localized inner shells of the atomic components.[9] Secondary electrons with initial kinetic energies up to about 20 eV turn out to be indeed the most abundant of the secondary species created by the primary ionizing radiation.[10] Recently, the ability of presolvated, free electrons to efficiently induce SSB and DSB effects in super coiled DNA has clearly been shown in several experiments.[11,12]

The experimental studies on inelastic electron processes with deoxyribose[5] in the gas phase, and the similar experiments on the D-ribose,[6] have both examined the fragmentation spectral appearances at near threshold energies, while only the deox-

[†] CASPUR, Supercomputing Consortium.
[‡] University of Rome La Sapienza.
[§] Texas A&M University.
[||] Freie Universitaet Berlin.
[#] Permanent address: Department of Chemistry, University of Podlasie, 08-110 Siedlce, Poland.

(1) Pigman, W.; Horton, D. *The Carbohydrates: Chemistry and Biochemistry;* Academic Press: New York, 1994.
(2) von Sonntag, C. *The Chemical Basis of Radiation Biology;* Taylor and Francis: London, 1987.
(3) Michael, B. D.; O'Neill, P. *Science* **2000**, *287*, 1603−1604.
(4) Boudaiffa, B.; Cloutier, P.; Hunting, D.; Huels, M. A.; Sanche, L. *Science* **2000**, *287*, 1658−1660.
(5) Ptasińska, S.; Denifl, S.; Scheier, P.; Märk, T. D. *J. Chem. Phys.* **2004**, *120*, 8505−8511.
(6) Bald, I.; Kopyra, J.; Illenberger, E. *Angew. Chem., Int. Ed.* **2006**, *45*, 4851.
(7) König, C.; Kopyra, J.; Bald, I.; Illenberger, E. *Phys. Rev. Lett.* **2006**, *97*, 018105.
(8) Grandi, A.; Gianturco, F. A.; Sanna, N. *Phys. Rev. Lett.* **2006**, *97*, 018105.
(9) Colson, A. O.; Sevilla, M. D. *Int. J. Radiat. Biol.* **1986**, *49*, 915.
(10) Cobut, V.; Fongillo, Y.; Patan, J. P.; Goulet, T.; Fraser, M. J.; Jay-Gerin, J.-P. *Radiant. Phys. Chem.* **1998**, *51*, 229.
(11) Sanche, L. *Eur. Phys. J. D* **2005**, *35*, 367.
(12) Martin, F.; Burrow, P. D.; Cai, Z.; Cloutier, P.; Hunting, D.; Sanche, L. *Phys. Rev. Lett.* **2004**, *93*, 068101.
(13) Schaftenaar, G.; Noordik, J. H. *J. Comput.-Aided Mol. Design* **2000**, *14*, 123−134.

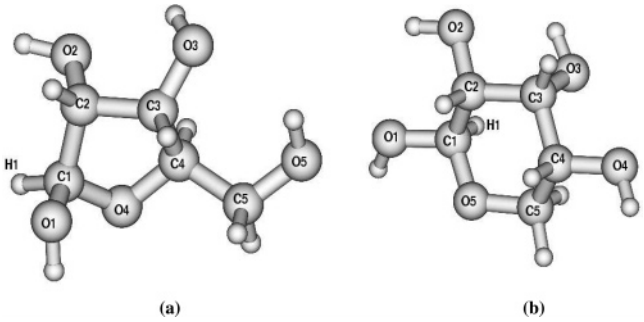

Figure 1. Optimized structure and atoms labeling for (a) the β-D-ribofuranose in and for (b) the β-D-ribopyranose. The figures were prepared using Molden.[13]

yribose data[5] have presented results at higher energies and fragmentation patterns up to about 10 eV. In the present work we therefore intend to report new experimental data on the higher-energy fragmentation patterns of D-ribose, together with a theoretical analysis of both the furanosic (Figure 1a) and the pyranosic (Figure 1b) ribose conformers (which are the most abundant structures of the ribose in the gas phase) to relate the measured fragmentation data with the presence of specific transient negative ions (TNIs) identified by our quantum scattering calculations. In supercoiled DNA, electrons at sub-excitation energies (<3 eV) only induce SSBs,[12] whereas electrons in the range 6−12 eV generate both SSBs and DSBs.[4,11] The higher-energy range discussed here is hence relevant for irreversible damage in living cells. We shall endeavor to show, therefore, that the spatial features of our computed resonant electrons, and their energy locations, indeed match what has been experimentally observed in terms of their locations and further suggest possible fragmentation pathways originating from the computed, metastable "doorway" states.

The work is organized as follows: the next section describes the new experimental findings on D-ribose while section 3 briefly reviews our computational machinery. Section 4 compares the computational results with the new and the earlier experiments on both D-ribose, while section 5 summarizes our conclusions.

2. Experiments on D-Ribose

The experiments on D-ribose were performed in an ultrahigh-vacuum chamber (base pressure 10^{-8} mbar) using a crossed electron/molecular beam with mass spectrometric detection of the generated ions.[14] The crystalline powder is housed in a vessel inside the chamber and is sublimated by heating the whole vacuum chamber to temperatures up to 370 K to prevent condensation on the surfaces. The electron beam is generated from a trochoidal electron monochromator[15] operated at an energy resolution of 100−120 meV fwhm at a current of ≈20 nA. The electrons intersect orthogonally with the effusive molecular beam and the generated ions are extracted by a small electric field toward the entrance of a quadrupole mass spectrometer (QMS) and detected by a secondary electron multiplier. The electron energy scale is calibrated using the well-known resonance of SF_6 generating metastable SF_6^- near 0 eV. All measurements were performed in the absence of the calibration gas to prevent ion−molecule reactions with the calibration gas. D-Ribose was obtained from Sigma Aldrich with stated purity of 98% and was used as delivered. To be sure that the sublimated D-ribose molecules are intact in the gas phase, the ratio of ion yields of heavy and light fragment ions have been determined upon further heating up to 410 K. This ratio was independent of the temperature, strongly indicating that in the relevant temperature range no thermal decomposition of the molecules takes place.

3. The Computational Procedure

3.1. Scattering Equations in a Single Center Expansion and Adiabatic Model. In the Born−Oppenheimer (BO) approximation one represents the total wave function of the "target + e^-" as an antisymmetrized product of electronic wave functions which depend on the positions of the nuclei. The scattering process under investigation is here initially limited to elastic channels and thus no further excitation channels are considered. We therefore analyze first a single nuclear geometry (the fixed-nuclei (FN) approximation), and the N bound electrons of the target are assumed to be in a specific molecular electronic state (ground state) which is taken to remain unchanged during the scattering. The target electronic wave function is given in the self-consistent field (SCF) approximation with a single-determinant description of the N occupied molecular orbitals (MOs). The occupied MOs are then expanded onto a set of symmetry-adapted angular functions with their corresponding radial coefficients represented on a numerical grid.[16,17]

By replacing the electronic exchange contribution with the energy-dependent local exchange potential suggested by Hara,[18] the ensuing scattering equations for the radial coefficients in the case of a closed-shell molecule take the form

$$\left[\frac{\mathrm{d}^2}{\mathrm{d}r^2} - \frac{l_i(l_i+1)}{r^2} + k^2\right] f_i^{p\mu}(r|\mathbf{R}) = 2\sum_j V_{ij}^{p\mu}(r|\mathbf{R})\, V_{ij}^{p\mu}(r|\mathbf{R}) \qquad (1)$$

where the asymptotic momentum k of the incident electron is given by $k^2/2 = E - \epsilon$, E is the total energy, ϵ is the electronic eigenvalue for the target asymptotic state at the nuclear geometry $\mathbf{R}$, and r is the radial coordinate of the scattering electron. The (p, μ) indices label the symmetry of the continuum wave function while the indices i or j represent an "angular channel" (l, h), h being one of the components of l.

We notice here that it is certainly possible that the correct exchange interaction might shift resonance energies, obtained by the complex poles of the scattering matrix **S**. However, the excellent qualitative agreement we have found between results obtained using an exact exchange and those given by the present local model exchange potentials when we analyzed isolated resonances in other systems (e.g., see ref 19) gives us confidence in assuming that the resonant trapping mechanism is likely to be the same for both potentials.

The dynamical short-range correlation is further included in the potential coupling elements of eq 1 through the addition of a local energy-independent potential which analytically depends on the density of the molecular target by means of a density-functional description of the correlation term.[16,20,21]

An alternative expansion basis to that of eq 1 is provided by the eigenfunctions obtained from diagonalizing the angular Hamiltonian at each radius r. These new angular eigenstates are referred to as the adiabatic angular functions (AAFs) $Z_k^{p\mu}(\theta, \phi, r)$ which are distance-dependent, linear combinations of the symmetry-adapted "asymptotic" harmonics mentioned before. The eigenvalues $V_k^A(r)$ of the angular Hamiltonian now form an adiabatic radial potential for each index value k over the selected range of the e^--molecule distances.[16]

(14) Balog, R.; Langer, J.; Gohlke, S.; Stano, M.; Abdoul-Carime, H.; Illenberger, E. *Int. J. Mass Spectrom.* **2004**, *233*, 267.
(15) Stamatovic, A.; Schulz, G. J. *Rev. Sci. Instr.* **1970**, *41*, 423.
(16) Lucchese, R. R.; Gianturco, F. A. *Int. Rev. Phys. Chem.* **1996**, *15*, 429.
(17) Altman, S. L.; Herzig, P. *Point-Group Theory Tables;* Oxford University Press: Oxford, 1994.
(18) Hara, S. J. *J. Phys. Soc. Jpn* **1967**, *22*, 710.
(19) Curik, R.; Gianturco, F. A.; Lucchese, R. R.; Sanna, N. *J. Phys. B* **2001**, *34*, 59.
(20) Perdew, J. P.; Zanger, A. *Phys. Rev. B* **1981**, *23*, 5048.
(21) Lee, C.; Wang, W.; Parr, R. G. *Phys. Rev. B* **1998**, *37*, 785.

Solving the scattering equations using these new $V_k^A(r)$ potentials allows the expansion of the scattering wave function in adiabatic angular states to converge more rapidly than the corresponding expansion in angular momentum eigenstates. Hence, the numerical instabilities in the solution of the standard momentum eigenfunction expansion when very large angular momentum values have to be considered (as in the present molecules) are greatly reduced.

To avoid the nonadiabatic coupling terms, we actually employ a piecewise diabatic (PD) representation for the potential[16] where the radial coordinate is divided into a number of regions. In each radial region we average the coupling potential $V_{l'h',lh}(r)$ over r, and the resulting averaged potential is diagonalized to yield a set of angular functions $Z_{k,i}^{p\mu}(\theta, \phi)$ for each region i thereby transforming the scattering potential into a new representation in which it is nearly diagonal. The resulting equations are then solved using the full scattering potential in each region with the further approximation of ignoring the off-diagonal couplings within the region (for further details see ref 16). (For a detailed discussion of our theoretical precedure when applied to biological systems we refer the reader to ref 22 and references therein.)

3.2. Resonances and Fragmentation Channels. Once the complex poles of the **S**-matrix, $E - i\Gamma/2$, are calculated in the selected energy range, we carry out a semiquantitative analysis to unravel the expected fragmentation dynamics following the formation of the TNIs (resonances) associated to each pole. Such analysis is essentially based on (1) the characterization of each **S**-matrix pole as an observable resonant state through the calculation of its lifetime, (2) the calculation of the vibrational normal modes of the neutral target molecule and of their corresponding periods, and (3) the analysis of the wavefunction and density maps associated to each resonance to extract a predicted pattern of fragmentation.

First of all, from the calculated Γ value which corresponds to the width at half-height of the resonant peak (for pure resonances), the lifetime τ is calculated as $\tau = h/\Gamma$, where Γ is given in eV and the Planck constant $h = 4.13566743 \times 10^{-15}$ eV·s. From the τ values we can locate each resonance in the range which goes from the impulse limit to the compound limit (see refs 23 and 24 for the earliest reviews on this topic). Such limit is associated to a direct (elastic) scattering process with no formation of metastable states. On the other hand, a (negative) compound state is formed if the electron resides around the molecule longer than $\sim 10^{-14}$ s, that is, longer than the typical period of a molecular vibration. Such lifetime allows for one or more molecular vibrations to take place before the compound decays (by autoionization, fragmentation, or decay to a stable anionic bound state with photon emission). For the fragmentation to take place there must occur an energy transfer from the incident electron's motion to the nuclear degrees of freedom, a transfer which depends on the efficiency of the vibronic coupling: the longer the excess electron stays around the molecule, the higher the probability for the energy transfer to take place.[23] In the intermediate situations between the impulse and the compound limit a quasi-bound state is formed, but the lower the lifetime is the faster the energy transfer must be for the fragmentation to be observed; that is, an efficient coupling between the electronic and the vibrational motions is required. From a qualitative point of view, we may expect such a condition to be verified for vibrational motions with periods smaller than or similar to the resonances lifetimes.

Following the previous argument, to qualitatively assess the possibility of an energy transfer during the lifetime of each resonance, we have performed the complete vibrational analysis of the neutral, molecular target. Here we assume that the TNIs' slow nuclear motion is adiabatically unperturbed, on the short time scale, by the change in the electronic structure owing to the attachment of the colliding electron; in other words, we assume that on the very short time scale, the anionic potential surface can be approximated, at least in the neighborhood of the neutral's equilibrium geometry, by shifting the neutral's surface upward in energy by the kinetic energy of the incident electron.[25]

For each of the $(3N - 6)$ normal modes we calculate the vibrational frequency $\tilde{\nu}$ (cm^{-1}) and the associated period $T = (1/\tilde{\nu}c)$, where the velocity of light in vacuum is given by $c = 2.99792458 \times 10^{10}$ cm·s^{-1}. Each mode can be analyzed in terms of the molecular motions (in internal coordinates) which describe the harmonic normal vibration.[26] The potential energy distribution (PED) of the normal modes relevant to a given resonance lifetime then permits to uniquely assign the internal coordinates subset involved in the vibrations. The comparison between the resonance lifetimes, τ, and the vibrational periods, T, suggests which nuclear motions (internal coordinates) are more likely to be involved in the vibronic energy transfer that can take place during the TNIs' formation. In particular, we consider the coupling will be effective for those nuclear motions whose periods are at most 1 order of magnitude larger than the resonances lifetimes. As mentioned above, if the TNI lives less than the time necessary for an entire vibration to be completed, only a fast energy transfer can cause bond-breaking effects. Hence, even though our analysis will point out specific fragmentation patterns for each resonance, in the case of short living TNIs such channels will be observed only in case of a sizable strength of the vibronic coupling. In the FN approximation we cannot evaluate such quantity. Hence, we can only indicate what transfers are most likely to take place from the comparison of T with τ and from the associated analysis explained below, thereby suggesting possible emerging fragments.

We finally plot the density and the wavefunction for the resonance states since such maps provide an extremely useful additional piece of information by showing where the excess electron energy in the TNI is localized with respect to the molecular skeleton. Frome them we can further identify regions with significant antibonding character which may be associated with the reaction coordinates in the ensuing TNI's fragmentation.[27] A significant antibonding character of the TNI wavefunction along some nuclear coordinates also corresponds, in the density map, to the existence of zero-density planes and marked gradients in the density function around that plane.

Gathering all the above information we can sketch our procedure to be as follows:

(1) We identify the most likely energy transfer channels (from the excess electron to the nuclear motions) as coming from the coupling to those normal modes which (i) vibrate on a time scale comparable to the resonance lifetime and which (ii) show a significant "overlap" between the nuclear and the resonance electronic wavefunction. The significant overlap is determined by the comparative analysis of the molecular regions involved in a particular normal mode with the density map associated to that resonance state.

(2) Once the excess electronic energy is transferred to the nuclear motion the fragmentation can proceed via the bonds along which the resonance wavefunction shows a significant antibonding character.

4. Results and Discussion

4.1. Experimental Findings. The experimental results in Figure 2 show the main fragmentation species observed in a broad energy range between around 5.0 and 9.5 eV, together with the strong threshold peaks already presented and discussed before.[6]

(22) Baccarelli, I.; Gianturco, F. A.; Grandi, A.; Lucchese, R. R.; Sanna, N. *Adv. Quantum Chem.* **2007**, *52*, 189.
(23) Chutjian, A.; Garscadden, A.; Wadehra, J. M. *Phys. Rep.* **1996**, *264*, 393.
(24) Schultz, G. J. *NSRDS-NBS;* U.S. Department of Commerce: Washington, DC, 1973; Vol. 50
(25) Anusiewicz, I.; Sobczyk, M.; Berdys-Kochanska, J.; Skurski, P.; Simons, J. *J. Phys. Chem. A* **2005**, *109*, 484.
(26) Fuhrer, H.; Kartha, V. B.; Kidd, K. L.; Kruger, P. J.; Mantsch, H. H. *Computer Program for Infrared and Spectrometry, Normal Coordinate Analysis;* National Research Council: Ottawa, Canada, 1976; Vol. 5.
(27) Illenberger, E.; Momigny, J. *Gaseous molecular ions: an introduction to elementary processes induced by ionization;* Springer: Darmstadt, Germany, 1992.

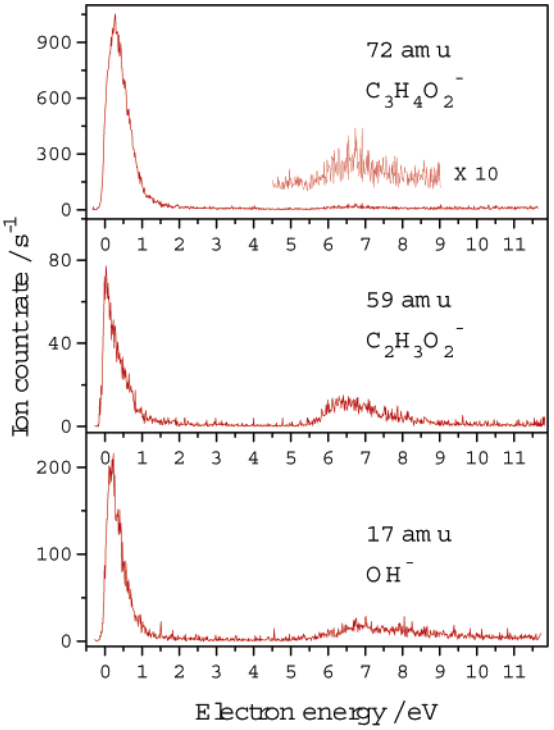

Figure 2. Ion yields from D-ribose at 72 amu (top panel), 59 amu (middle panel), and 17 amu (bottom panel). The molecular structures corresponding to each fragment are also reported. The threshold peak has been analyzed in ref 6.

These threshold signals are present in D-ribose,[6] deoxyribose,[5] and fructose[28] with the common feature that the corresponding fragment anions are due to the loss of one or more neutral water molecules but also C-containing neutral fragments arising from the degradation of the ring structure. In D-ribose it was demonstrated[6] by means of isotope labeling that the reactions induced at very low energies (near zero eV) are subjected to a remarkable selectivity in the way that every anionic fragment contains the C1 atom (see Figure 1). This is shown in Figure 3for the light fragment anion at 59 amu ($C_2H_3O_2^-$) which represents either an enol-like compound (HO)HC═CHO$^-$ or the acetate anion CH_3COO^-. Irrespective of the detailed structure of this fragment, it must arise from a breakup of the ring. Labeling at the C1 position (1-^{13}C-ribose) results in a shift of about 80% of the intensity from 59 to 60 amu indicating that 80% of the fragment ions contain 1-^{13}C. In a statistical decay of the transient anion one would expect that 40% of the fragment ions contain 1-^{13}C.

Complementary to that, Figure 3 also shows the result of the labeling at C5 (5-^{13}C-ribose) indicating that more than 80% of the intensity remains at 59 amu, that is, the neutral fragment at a high selectivity contains the 5-^{13}C atom. Accordingly, deuteration at the 1-C position (*C*, 1-D-ribose, in the enumeration of Figure 1 this is H1) indicates that more than 50% of the fragments contain the deuterium which is appreciably above the ratio one would expect from a statistical decomposition of the transient anion. From that it can be concluded that (i) the transient anion giving a two-carbon fragment possesses a remarkable tendency to involve the C1 atom and (ii) there is no hydrogen scrambling during decomposition of the TNI.

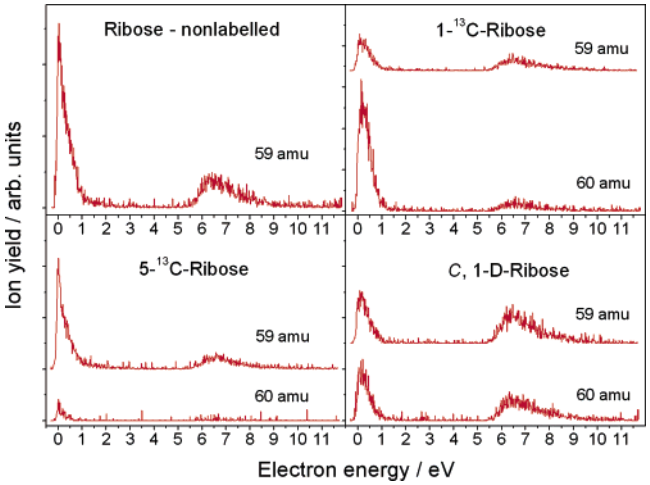

Figure 3. Ion yields at 59 and 60 amu, respectively, obtained from different isotope labeled D-ribose samples.

From Figure 3 it can directly be seen that the feature at higher energy does not show such a pronounced localization of the excess charge on C1 as both 1-^{13}C-ribose and *C*, 1-D-ribose appear at 59 and 60 amu at comparable intensities. As our calculations will show, this feature can be assigned to four shape resonances each having characteristic antinodal planes across C−OH and C−C bonds which can be associated to OH^- formation but also to fragment anions originating from the ring break as observed in the experiment. It should further be noted that at these energies, core excited resonances may also contribute to the fragment ions observed.

4.2. Analysis of the *β*-D-Ribofuranose. As mentioned above isotopic labeling of D-ribose enables one to identify the underlying processes and to suggest specific sites involved in the fragmentation reaction at those energies. In the present calculations we shall show that the higher-energy region can be associated with specific shape resonances found from the scattering model employed here.

The electronic structure calculations describing the target furanosic structures were obtained using a single determinant (SD) description of their optimized geometries carried out at the 6-31G* quality of the basis set expansion (see Figure 1a for the atoms labeling in the optimized *β*-D-ribofuranose). The SCE subsequent expansion of the bound orbitals was carried out up to $l_{max} = 40$, while the corresponding interaction potential was expanded up to $\lambda_{max} = 80$. The ensuing components of the diabatic potentials were extended up to $l_{max} = 9$, and the radial integration range went out to $R_{max} = 13.5$ a_0. The angular grid (ϑ, φ) included a total of 492 points and the search for the poles in the **S**-matrix which identify the resonances was carried out by varying the above parameters to ensure convergence of the energy and width values within 5%.

One should be aware of the fact that a considerable amount of computational results have been reported on the deoxyribose radical, the radical cations, and some structurally related compounds by looking at radical stability, charge localization, and charge transfer following DNA irradiation.[9,29,30] Furthermore, the minimum energy conformations of the ribose and the ribose radicals from H-abstraction were determined from the

(28) Sulzer, P.; Ptasinska, S.; Zappa, F.; Mielewska, B.; Milosavljevic, A. R.; Scheier, P.; Märk, T. D.; Bald, I.; Gohlke, S.; Huels, M. A.; Illenberger, E. *J. Chem. Phys.* **2006**, *125*, 44304.

(29) Antic, D.; Parenteau, L.; Sanche, L. *J. Phys. Chem. B* **2000**, *104*, 4711.
(30) Barrios, R.; Skurski, P.; Simons, J. *J. Phys. Chem. B* **2002**, *106*, 7991.

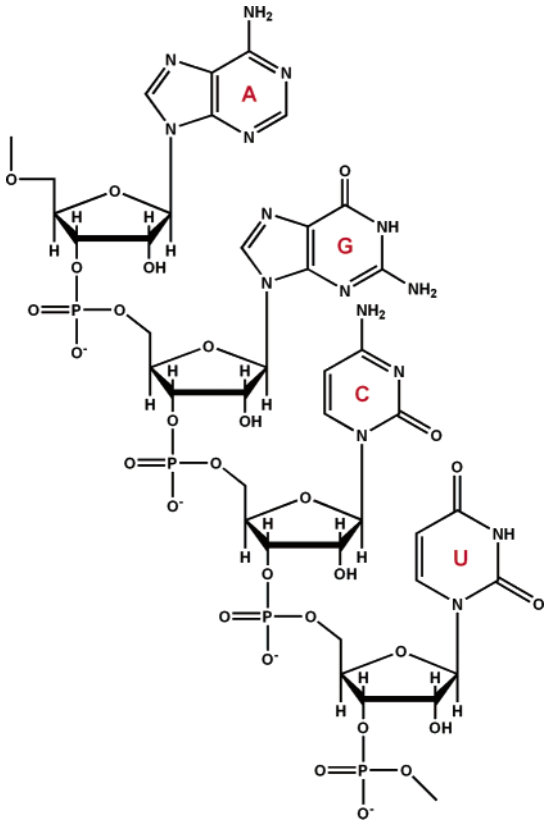

Figure 4. A simplified pictorial representation of the RNA strand through the presence of its building blocks. The furanosic sugar rings are clearly shown.

ab initio method[31] with a small preference for H abstraction from the C adjacent to the alicyclic O observed for the furanose ring.[32] Additional theoretical investigations have also looked at several properties of a variety of DNA components, like electron affinities, ionization energies, etc., also including the ribose and deoxyribose fragments.[33−35]

In each nucleotide monomer defining the RNA structure, the ribose unit is present as a furanose ring structure of five atoms with the C1 position connected to the various bases through the glycosidic C−N bond and with the C5 position bound to the phosphate group through the C−O bond. The nucleotide formation therefore occurs from its building blocks (bases-sugar molecules-phosphate groups) by a condensation reaction which releases two water molecules. To pictorially exemplify this structure we show in Figure 4 the sequential attachments of the four bases to the (sugar−phosphate) RNA backbone.

We have searched for resonances through the analysis of the poles of the **S**-matrix in the complex plane and have selected the roots with complex part, Γ/2, smaller than 2 eV, corresponding to resonances with lifetimes longer than 1 fs. In Table 1 we report the position, the width, and the lifetime for the resonances found in the range 0−11 eV for the ribose molecule in the furanosic form. Even though none of the resonances can be characterized as a long-lived compound state, the τ values nevertheless show that such poles actually describe the metastable attachment of an electron to the molecular framework; in fact, the corresponding lifetimes are longer than for an impulse encounter. We have further represented the spatial features of the excess, $(N + 1)^{th}$ electron associated with each TNI by mapping the real part of the single-particle scattering wavefunction and the corresponding density over the physical space of the molecular nuclei at their equilibrium geometries, as will be discussed later on.

Table 1. Position (in eV), Width (in eV), and Associated Lifetime (in s) of the Transient Negative Ions Found for the β-D-Ribofuranose Molecule in the Range 0−11 eV

E (eV)	Γ (eV)	τ (s)
6.41	0.90	4.60×10^{-15}
8.46	1.93	2.14×10^{-15}
9.48	2.41	1.72×10^{-15}
10.63	2.37	1.75×10^{-15}

Table 2. HF/6-31G* Frequencies (in cm^{-1}) and Periods (in s) of the D-Ribose Normal Modes Together with Their Characterization in Terms of Molecular Vibrations[a]

mode number	$\tilde{\nu}$ (cm^{-1})	T (s)	mode type
$\nu_1-\nu_{18}$	59−854	5.70×10^{-13}− 3.91×10^{-14}	δ ring
$\nu_{19}-\nu_{44}$	912−1675	3.66×10^{-14} − 1.99×10^{-14}	δ ring + ν ring
ν_{45}	3188	1.05×10^{-14}	ν (C−H)
ν_{46}	3239	1.03×10^{-14}	ν (C−H)
ν_{47}	3248	1.03×10^{-14}	ν (C−H)
ν_{48}	3273	1.02×10^{-14}	ν (C−H)
ν_{49}	3285	1.02×10^{-14}	ν (C−H)
ν_{50}	3291	1.01×10^{-14}	ν (C−H)
ν_{51}	4074	8.19×10^{-15}	ν (O3-H)
ν_{52}	4085	8.17×10^{-15}	ν (O5-H)
ν_{53}	4096	8.14×10^{-15}	ν (O1-H)
ν_{54}	4117	8.10×10^{-15}	ν (O2-H)

[a] The labels refer to the numbering of the atoms in Figure 1a, δ = bending, ν = stretching.

Following the procedure sketched in the previous section, to analyze the relevant dynamics of fragmentation of the TNIs we characterized the entire vibrational spectrum of the D-ribofuranose in the harmonic approximation. The analysis has been carried out with the Gaussian package[36] at the HF/6-31G* level, coherently with the electronic structure calculation described above. The frequencies, periods, and assignment of all the 54 normal modes of the D-ribose molecule are reported in Table 2.

By comparing the vibrational periods with the TNIs lifetimes we notice that all the resonances live long enough for the ribose faster vibrations (associated from PED analysis to ν(OH) stretchings, see Table 2) to take place, even though the lifetimes do not allow for a complete vibration to occur. Hence, for such times it should be likely to have an efficient coupling between the excess electronic wavefunction and the O−H vibrations, provided the resonant states also have a non-negligible electronic density in the molecular regions interested in such vibrations. By plotting the real part of the wavefunction and the density of the excess $(N + 1)^{th}$ electron we can first of all associate to each TNI the vibrational mode which exhibits a significant overlap with respect to the electronic wavefunction; finally, by

(31) Miaskiewicz, K.; Osman, R. *J. Am. Chem. Soc.* **1994**, *116*, 232.
(32) Fitshett, M.; Gilbert, B. C. *J. Chem. Soc. Perkin Trans.* **1988**, *2*, 673.
(33) Younkin, J. M.; Smith, L. J.; Compton, R. N. *Theor. Chim. Acta* **1976**, *41*, 157.
(34) Oyler, N. A.; Adamowicz, L. *J. Phys. Chem.* **1993**, *97*, 11122.
(35) Wetmore, S. D.; Boyd, R. J.; Eriksson, L. A. *Chem. Phys. Lett.* **2001**, *343*, 151.
(36) Frisch, M. J.; et al. *Gaussian 03*, revision C.02; Gaussian, Inc.: Wallingford, CT, 2004.

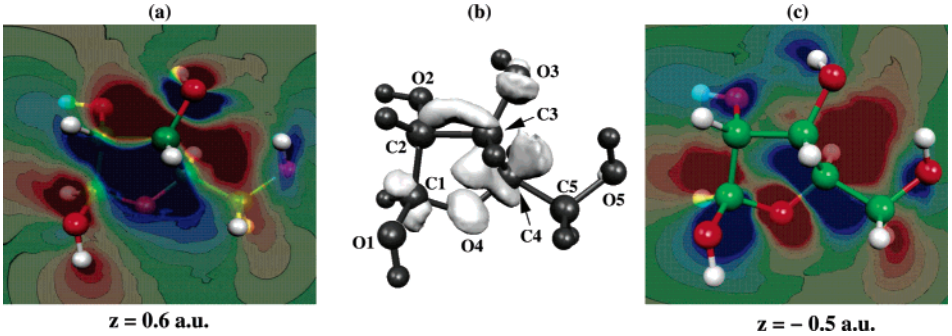

Figure 5. Contour plots (at (a) $z = 0.6$ au and at (c) $z = -0.5$ au) and density map for the computed resonant state at 6.41 eV (b). All contour plots and density maps here and in the following figures were prepared using Molekel 4.0.[37]

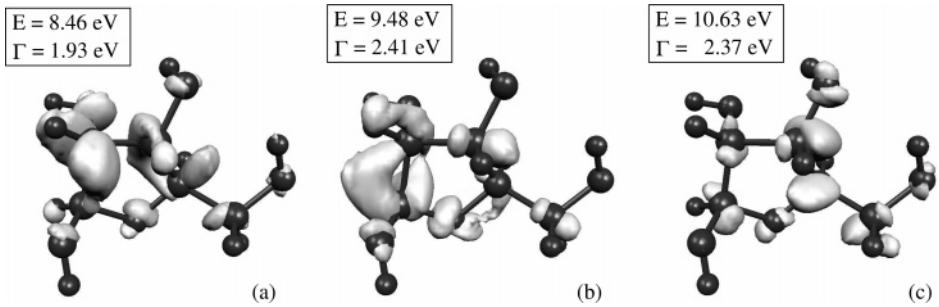

Figure 6. Density maps for the second, third, and fourth TNIs of the β-D-ribofuranose.

the analysis of the antibonding features in the resonance functions we can suggest the most likely fragmentation patterns.

In Figure 5 we report in panel a the contour plot for the real part of the scattering wavefunction ($\Psi_{res}^{real}(x, y, z)$) and in panel b the density $|\Psi(x, y, z)|^2 = (\Psi_{res}^{real})^2 - (\Psi_{res}^{im})^2$ of the first resonance state. The contour plot is a two-dimensional cut of the wavefunction taken along the plane $z = 0.6$ au (the origin of the reference system is in the center of mass, and the plane $z = 0$ is at the ring level) and lies along the C3−O3 bond (see Figure 1a for the atom numbering). The density plot shows the excess electron mostly delocalized over the ring and on one of the four O−H bonds, namely the O3-H. We can thus suppose the energy transfer from the electronic to the vibrational motion to occur via the coupling to the vibrational mode ν_{51} (see Table 2) which shows both a comparable period on the time scale and a significant overlap with the first TNI of the ribofuranose. From the contour plot in the left panel of Figure 5 one can easily notice the antibonding character of the C3−O3 bond, along which the electronic wavefunction presents a nodal plane. Concerning the first resonance state (at $E = 6.41$ eV) we can hence conclude that (i) the most likely energy transfer from the electronic to the nuclear motion occurs via the coupling to one of the O−H vibrations, namely to the ν_{51} mode; (ii) the antibonding features of the corresponding TNI suggests the break of the C3−O3 bond with the release of an OH^- fragment in an excited vibrational state:

$$C_5O_5H_{10} + e^- \rightarrow (TNI)^* \rightarrow (C_5O_4H_9)^\bullet + (OH^-)^* \quad (2)$$

The first resonance is the one showing the longest lifetime and hence the best possibility to efficiently couple with lower frequencies (slower motion) vibrational modes. In particular, the modes associated to ring stretchings ($\nu_{19}-\nu_{44}$) vibrate on a time scale which is less than 1 order of magnitude longer than the first resonance's lifetime (see Table 1). Hence, the first TNI might also undergo fragmentation involving the ring break with possible releases of O^- from the ring (the O4 atom) which presents sizable excess charge (see Figure 5) and antibonding characters along the O4−C4 and the O4−C1 bonds (see in Figure 5c the contour plot at $z = -0.5$ au, i.e., along the plane cutting such bonds). By analyzing the density map and the contour plots along different planes it is also possible to suggest other fragmentation channels, but the great amount of vibrational modes relative to ring stretchings makes it more difficult to identify more specifically the most likely bond breaks at the present level of analysis.

The density maps for the other three resonances found in the 5−11 eV range are reported in Figure 6. Again, we look for electron localization on one (or more) OH bonds (the "fast" vibrators with respect to the resonance lifetimes) to identify the most likely couplings and energy transfers to nuclear motions. The second TNI (Figure 6a) shows a relevant localization of the electronic wavefunction on the O2 atom which is involved in the O−H vibration characterizing the ν_{54} mode. Again, the contour plot (not reported for sake of brevity) shows a marked antibonding character in correspondence of the C2−O2 bond, suggesting the possible decay of the TNI with the release of an excited negatively charged OH fragment according to eq 2, the difference with the decay of the first TNI being given by a different $(OH^-)^*$ fragment released in the environment.

The third TNI (Figure 6b) shows a favored coupling to the ν_{53} mode owing to the partial localization of the excess electron on the O1 atom and an antibonding character along the C1−O1 bond. Finally, the fourth TNI (Figure 6c) indicates the ν_{51} and the ν_{52} as the most likely vibrational motions involved in the energy transfer and the presence of antibonding character on both the C3−O3 and the C5−O5 bonds. Again, the third and fourth TNIs can be seen as precursors of molecule

(37) Flukiger, P.; Luthi, H. P.; Portmann, S.; Weber, J. *MOLEKEL 4.0*; Swiss Center for Scientific Computing: Manno, Switzerland, 2000.

fragmentation with the release of a negatively charged OH fragment in some excited state (eq 2).

If we look at the four TNIs found by the calculations for the D-ribofuranose molecular system, we would expect to be able to distinguish two peaks in the fragmentation spectrum relative to the OH^- detachment (lowest panel in the experiments in Figure 2), this being the decay channel common to all four TNIs. The first peak would be associated to the narrower resonance at 6.4 eV while the second would result from the combination of the other three resonances extending from about 7.4 up to 11 eV. However, from the values of positions and widths reported in Table 1 we also notice that the first two resonances nearly overlap; indeed, even though the lowest panel of Figure 2 shows some complex structure between 6 and 9 eV it is not possible to clearly identify two different peaks. In any case, the energy range of the computed resonances is remarkably close to the one shown by the experiments reported by Figure 2 where the high-energy features of the ion yield extend exactly over the same range of energies found by our calculations. We could therefore argue that our four resonant features model the relevant shape resonances which act as doorway states for the fragmentation patterns detected by the experiments on this molecule. Furthermore, our combined analysis of the molecular vibrational modes and of the resonant wavefunctions points at the detachment of OH^- (lowest panel in the experiments in Figure 2) that might take place as a direct fragmentation of such bonds, where excess negative charge also remains located over that chemical fragment.

With the same token, we also find that in the first resonant wavefunction there is a clear location of excess charge over the furanosic ring and that such quantum charge distribution further exhibits antibonding planes across some of the C−C bonds of the ring. It therefore becomes plausible to suggest that the two further fragments reported by the experiments in the panels of Figure 2 could also originate from the direct fragmentation of these antibonding regions of the sugar ring with the formation of residual fragments with either two or three carbon atoms and the ensuing loss of the lighter H atoms along dissociation. However, the identification of the fragments is in this case less straightforward because of the greater complexity of the vibrational spectrum in this frequency range; to have a semiquantitative analysis of the fragmentation patterns a further analysis of the potential energy features as a function of internal coordinates would be needed.

One should also note, however, that we cannot exclude the possibility that all the higher-energy fragmentations could originate from a mechanism which is not only a direct bond-breaking along antibonding surface lines but is also due to the presence of an initial core-excited transient state which does not appear in our calculations. The fact that our calculations do envisage the presence of trapping resonances in that energy range, and are able to attribute to the corresponding excess electrons specific spatial features which do not occur in the occupied MOs, does not exclude the additional role of Feshbach resonances but does suggest the likelyhood of forming "doorway states" from the dynamical electron trapping by shape resonances at equilibrium geometries.

4.3. Analysis of the β-D-Ribopyranose. One interesting issue which is opened up by the experiments being carried out in the gas phase is that of the actual geometries which are present during the electron scattering process. Thus, while the RNA building blocks exhibit β-D furanosic structures within the double helix, the isolated gas-phase species were found to be prevalently given[38] by a lowest-energy configuration represented by the pyranosic form. It therefore becomes interesting to carry out additional calculations with the latter spatial geometry (i.e., the β-D-ribopyranose structure) to see possible effects of such structural changes on the resonance shapes and locations.

Table 3. Position (in eV), Width (in eV), and Associated Lifetime (in s) of the Transient Negative Ions Found for the β-D-Ribopyranose Molecule in the Range 0−11 eV.

E (eV)	Γ (eV)	τ (s)
7.98	1.59	2.60×10^{-15}
8.23	2.84	1.46×10^{-15}
8.67	1.35	3.06×10^{-15}
9.49	3.14	1.32×10^{-15}

The analysis of the **S**-matrix poles relative to the electron scattering off the β-D-ribopyranose shows, as in the ribofuranose case, the presence of four resonance states in the range 0−11 eV with $\Gamma < 4$ eV, that is, with lifetime larger than 1 fs (see Table 3). Again, no resonance states are found at the threshold suggesting that the fragmentation channels experimentally observed at low energy should not be due to a trapping mechanism by the shape of the potential. The lowest energy TNI for the ribopyranose is somehow shifted at higher energies ($E = 7.98$ eV) with respect to the ribofuranose, whose first resonance state is located at $E = 6.41$ eV, and shows a shorter lifetime. However, the energy positions of the four TNIs are centered around 8 eV and exhibit widths of more than 1 eV, again matching the experimental findings of Figure 2 and 3.

The vibrational analysis for the ribopyranose offers a description of the nuclear motion very similar to what was found for the furanose conformer. The largest differences are observed for the lowest frequency modes (in the furanose: $\nu_1 = 59$, $\nu_2 = 121$, $\nu_3 = 136$, $\nu_4 = 216$, $\nu_5 = 257$ cm^{-1}; in the pyranose we find, respectively, 124, 149, 249, 276, and 282 cm^{-1}). The frequencies for the remaining 49 normal modes differ always less than 10%, with most differences around 1%. The description of the modes in terms of internal coordinates (see the 4th column in Table 2) is also the same, namely the first 18 modes correspond to ring bendings, the next 26 describe combinations of ring bendings and stretching, ν_{45} up to ν_{50} are C−H stretchings, and the last 4 modes correspond to O−H stretchings. Finally, the vibrational periods differ in a negligible way and, in particular, the highest frequency O−H vibrations have the same periods (around 8.1 fs). Hence, the resonances parameters (Table 3) and the vibrational analysis show that the analysis of the vibronic couplings and of the energy transfer efficiency discussed in the previous section hold for the ribopyranose as well.

To further look at the fragmentation patterns expected for the pyranose conformer, we report in Figure 7 the density map and two contour plots describing the first TNI, while in Figure 8 we report the density distributions relative to the second, third, and fourth TNIs. The maps show that the excess electron is not anymore "selecting" (at least for the first and third resonances) one single −OH fragment as it happened for the first three

(38) Guler, L. P.; Yu, Y.-Q.; Kenttamaa, H. I. *J. Phys. Chem. A* **2002**, *106*, 6754.

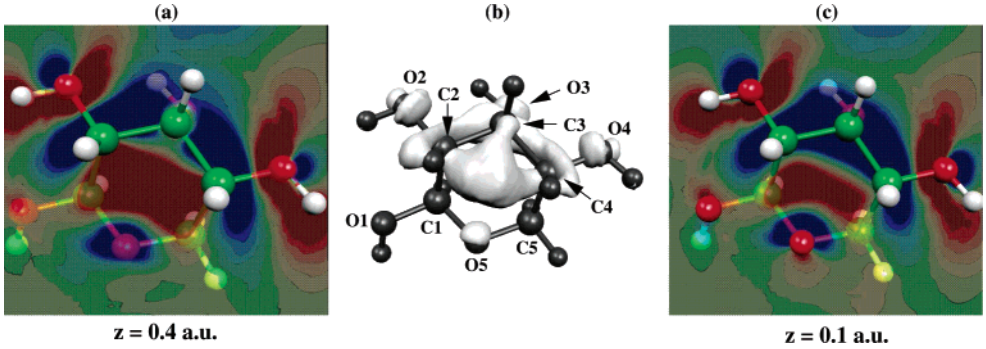

Figure 7. Contour plots (at $z = 0.4$ au (a) and $z = 0.1$ au (c)) and density map (b) for the ribopyranose resonant state at 7.98 eV. For the sake of clarity only some of the atoms are labeled.

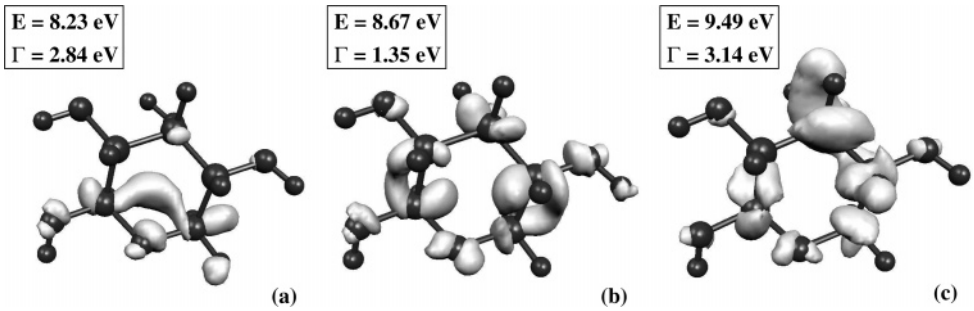

Figure 8. Density maps for the second, third, and fourth TNIs of the β-D-ribopyranose.

resonances of the ribofuranose (see before). In the first TNI of the ribopyranose the excess electron is localized on one part of the ring (around the C2−C3−C4 region) and on four out of the five oxygen atoms, namely on the ring oxygen O5 and on the three oxidrilic oxygen atoms O2, O3, and O4. Then, when we consider the oxidrilic regions, the second TNI shows a preferred electronic localization on the O1, the third TNI mainly on the O1 and O4 (but the O2 and the O3 also host some excess charge) and, finally, in the fourth TNI the O3 is favored with respect to the other oxidrilic oxygen atoms.

However, the main features of all the four furanosic resonances appear in the pyranose conformer as well; that is, (i) the lifetimes of the TNIs are comparable with the vibrational periods associated to the fast OH vibrations; (ii) all the four TNIs show some degree of electronic localization on one (or more) OH fragments, suggesting an efficient coupling of the electronic motion with those fast molecular modes; (iii) the C−OH bonds related to the "coupled" OH vibrations present a marked antibonding character which can ultimately lead to fragmentation with the release of vibrationally excited OH^- fragments. This is shown here only for the first resonance (for the sake of brevity) by means of the contour plots reported in the panels a and c of Figure 7. Figure 7a refers to a contour plot of the real part of the resonant wavefunction taken on the plane $z = 0.4$ au, which cuts through the C2−O2 and C4−O4 bonds and clearly shows the nodal planes exhibited by the wavefunction along such bonds. The same is true (though not reported here) for the C3−O3 bond.

In Figure 7c we also report the contour plot of the same function as in panel a taken this time on a plane nearer to the ring ($z = 0.1$ au), which cuts through the C1−C2 and the C4−C5 bonds. As in the furanosic case, the coupling of the excess electron motion in a resonant state with normal modes associated to ring stretchings is less favored, since such modes vibrate on a longer time scale with respect to the resonances' lifetimes. Moreover, it is less straightforward to identify (without a proper PED analysis) the contributions of single molecular fragments to assess the most likely coupling channels along specific internal coordinates. However, concerning the first resonance the Figure 7b and 7c would suggest that, if the energy transfer to the ring motion occurs, we would expect the release of a negatively charged molecular fragment with three carbon atoms (C2−C3−C4) or with two carbon atoms (C1−O5−C5):

$$C_5O_5H_{10} + e^- \rightarrow (\mathrm{TNI})^* \rightarrow (C_3H_xO_y)^- + (C_2H_{10-x}O_{5-y})^\bullet \quad (3)$$

$$C_5O_5H_{10} + e^- \rightarrow (\mathrm{TNI})^* \rightarrow (C_2H_{x'}O_{y'})^- + (C_3H_{10-x'}O_{5-y'})^\bullet \quad (4)$$

In a similar fashion we can suggest ring fragmentation decays of the higher-energy TNIs which would lead to the detection of only two- and three-carbon fragments in addition to the OH^- channel, resulting in a perfect agreement with the experimental findings reported in Figure 2. However such proposal on the ring fragmentation patterns would need further analysis of the nuclear motions which would constitute a work on its own and would go beyond the scope of the present work.

5. Conclusions

In this work we report experimental results for the fragmentation spectra in the higher-energy region (6−10 eV) for the gas-phase β-D-ribose molecule and furthermore carried out quantum dynamical calculations for their TNI formation both for its furanosic structure, as present in the RNA backbone structure, and for the pyranosic structure which was suggested to be the main stable configuration in the gas-phase.[38]

The new measurements indicate the presence of broad resonant states associated with OH^- fragmentation and with possible ring-breaking processes, all appearing in the region

between about 6 and 9 eV. The corresponding calculations identify four shape resonance structures exactly in the same energy range and associated with rather broad width values. The vibrational analysis of the neutral molecular target furthermore suggests the presence of efficient coupling between the excess electron motion in the resonance states and the faster vibrations associated with the -OH stretchings and, consequently, a possible energy transfer to the nuclear degrees of freedom. A further analysis of the density map and of the spatial nodal structures of the wavefunctions for the excess, metastable electron trapped during the resonant process reveals that the excess charge is indeed localized on the oxidrilic groups, on the ring oxygen, and on some of the carbon atoms of the furanosic ring and also shows that antibonding nodal planes exist both across the C−OH and across the C−C bonds of the ring. Thus, one could argue that possible decay channels which lead to OH^- and to molecular fragments originating from the ring break are likely to have the present TNIs as doorway states and to occur along repulsive potential energy surfaces involving the above bonds.

Our calculations for the ribose molecule do not indicate any resonant structures near threshold, a finding in accord with the recent calculations at the static-exchange level on the related deoxyribose carried out with an entirely different dynamical model.[39] Since the experiments, on the other hand, reveal intense signals from threshold and up to about 1.0 eV[5−7] leading to hydrogen and water molecule abstractions, among other processes, one can argue that such resonances do not have simple dynamical trapping (shape resonances) as their doorway states but rather more complicated low-energy reactions possibly amplified by single/double core-excited, Feshbach-type resonances that would need a post-SCF description of the target molecule. In other words, the presence of computed shape resonances, or their absence, can be used to identify (or to exclude) at the nanoscopic level specific, initial TNI formation processes leading to that fragmentation pattern which is experimentally observed. It does not tell us, however, on the possible presence of other resonant mechanisms which could be cooperatively active at those energies.

Furthermore, the calculations on the pyranosic (six-member ring) structure suggested by earlier work[38] to be the more stable structures in the gas-phase, reveal that the qualitative features of the TNIs are not modified from those of the furanosic structure while their widths remain broad enough to also match the experimental results.

In conclusion, the present study suggests that the furanosic blocks of the RNA backbone are indeed sensitive to electron attachment processes and can undergo irreversible damage with energetic electrons up to about 10 eV, with obvious direct consequences on the lethal effects of these secondary projectiles on the RNA structures and on the occurrence of strand breaks after the interaction. Their computed widths, however, turn out to be fairly broad and do not suggest the presence of electron residence times on the sugar blocks long enough to justify their transfer to either the nucleic bases or the phosphate backbone. Their break-up, therefore, could be more efficiently induced by direct electron attachment to such species and we are currently completing additional theoretical and experimental work to clarify this point.

Acknowledgment. The financial support of the MUIR, Ministery for University, Industry and Research, of the Scientific Committee of the University of Rome "La Sapienza", of the Deutsche Forschungsgemeinschaft and the computational support of the CASPUR Supercomputing Consortium are gratefully acknowledged. The FIRB programme is also acknowledged for financial support. F.A.G. thanks the Alexander von Humboldt Stiftung for the award of a visiting fellowship to the Free University of Berlin during the years 2004−2006, I.B. is fellow of the Studienstiftung des deutschen Volkes, and J.K. acknowledges support from polish scientific funds for the years 2005−2007 by the Grant No. 3T09A11129 and support for a visit to Berlin by the EU program COST (Co-Operation in the Field of Scientific and Technical Research).

Supporting Information Available: Complete ref 36. This material is available free of charge via the Internet at http://pubs.acs.org.

JA070542H

(39) Winstead, C.; McKoy, V. *J. Chem. Phys.* **2006**, *125*, 074302.